Applied Energy 339 (2023) 120955

Contents lists available at ScienceDirect

Applied Energy

journal homepage: www.elsevier.com/locate/apenergy

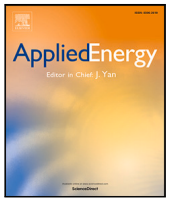

Optimal sizing and siting of energy storage systems considering curtailable photovoltaic generation in power distribution networks

Rahul Gupta [a,*], Fabrizio Sossan [b]

[a] Distributed Electrical Systems Laboratory, EPFL, Switzerland
[b] School of Engineering, Institute of Sustainable Energy, HES-SO Valais-Wallis, Switzerland

ARTICLE INFO

Keywords:
Energy storage systems
PV generation
Curtailment
Optimal planning

ABSTRACT

This work proposes a method for optimal planning (sizing and siting) energy storage systems (ESSs) in power distribution grids while considering the option of curtailing photo-voltaic (PV) generation. More specifically, for a given PV generation capacity to install, this method evaluates whether curtailing PV generation might be more economical than installing ESS. Indeed, while curtailing excess PV generation might be considered a last resort to avoid grid violations during operations, it is typically neglected in the planning phase. The proposed method accounts for the constraints of the power grid (i.e., nodal voltages, lines, and substation transformer limits) modeled by linearized power flow equations to keep the problem formulation tractable. The planning problem minimizes the net investment costs of the ESSs, and the imported and exported electricity costs considering a planning horizon of 20 years. The results are presented for a medium voltage (MV) distribution grid with different levels of installed capacity of PV generation, reflecting future scenarios of PV generation development. The sensitivity of the ESSs' sizes and investment costs to the electricity prices accounting for variable levels of PV production in the global generation mix is also investigated.

1. Introduction

Given the prominent role of photo-voltaic (PV) generation for meeting fossil-free energy-transition targets, it is to be expected that power distribution grids will host significant levels of PV generation in the future. High levels of PV generation in distribution grids can cause violations of statutory voltage levels, congestions in lines and substation transformers, especially when the generation largely exceeds the nominal demand.

In the existing literature, several methods have been proposed to solve these problems, such as curtailing excess PV generation [1,2], installing energy storage systems (ESSs) [3–5], and reinforcing existing power lines and transformers [6,7]. The works in [1,8–11] have shown that curtailing excess PV generation is economically and technically viable. The works in [12,13] proposed to limit PV generation passively or actively to curb reverse power flows. In [14], a fixed limit on the household export was imposed, whereas a percentage of the installed capacity was allowed to be curtailable in [12]. An overview of global trends on the acceptance of curtailment strategy is presented in [11].

Installing ESSs to support the grid operations has also been widely investigated [3,15–20]. For example, planning ESSs for voltage regulation was proposed in [15–17], for frequency regulation in [18,19], and for lines and transformer congestion management and minimizing reverse power-flows in [3,20]. In these works, the PV plants are modeled as uncontrollable power injections without the possibility of curtailing any power; not exploring the potential trade-offs between ESSs and PV curtailment might result in large, and possibly sub-optimal, energy storage capacity requirements.

The works in [8,10] explored curtailing PV generation in combination with controlling ESSs without, however, considering the grid's constraints. Authors of [1,14] defined export limits from PV plants including curtailment and grid constraints using optimal power flows (OPFs) and Monte-Carlo methods, however without considering ESSs. The work in [9] proposed combined strategic sizing of PV plants and ESSs in LV grids considering the investment costs, PV curtailment, and substation transformer capacity. The work in [21] proposed a rule-based method to plan distribution grids (including grid reinforcements) considering the PV curtailment option, however without ESSs.

In summary, planning formulations from the existing literature either ignore the grid constraints or do not consider curtailing PV generation in combination with optimal sizing of ESSs.

In order to fill this gap, this paper proposes a method to size and site ESSs in distribution grids while considering PV curtailment and distribution grid's operational constraints, namely nodal voltage limits,

* Corresponding author.
E-mail address: rahul.gupta@epfl.ch (R. Gupta).

https://doi.org/10.1016/j.apenergy.2023.120955
Received 11 November 2022; Received in revised form 10 February 2023; Accepted 5 March 2023
Available online 21 March 2023
0306-2619/© 2023 The Author(s). Published by Elsevier Ltd. This is an open access article under the CC BY license (http://creativecommons.org/licenses/by/4.0/).

lines' ampacities, and substation transformers' ratings. Studying sizing and siting of ESSs, in combination with curtailment of PV generation for satisfying the grid constraints stands as the main contribution of this paper. The grid constraints are modeled with a linearized power flow model, achieving a tractable formulation compared to traditional non-linear AC optimal power flow models. We use a linearized power flow model because it can be applied to distribution grids with both radial and meshed configurations, as opposed to second-order cone relaxations that are typically valid for radial systems [22,23].

The proposed planning method is applied to a medium voltage (MV) distribution grid; the results of the ESS planning with and without the PV curtailment options are discussed. In addition, assuming a scenario where PV generation is the dominant source of production at the system level, we perform a sensitivity analysis on the electricity price aimed at exploring the difference in the resulting ESSs' plans when PV is curtailed.

The paper is organized as follows. Section 2 describes the problem and the proposed methods, Section 3 presents the case study, and Section 4 presents and discusses the results. Finally, Section 5 draws the main conclusions.

2. Problem formulation

We consider a distribution network interfacing prosumers with electrical demand and distributed PV generation: the objective of the problem is to determine the cost-optimal sites and sizes (i.e., converter's power rating and energy storage capacity) of ESSs to satisfy the grid's operational constraints while considering optional PV curtailment. The problem accounts for the investment costs for the ESSs and the total running costs of all resources in the distribution grid, given by the difference between the cost of consumed electricity and the revenues from selling PV energy to the grid. The problem is formulated as a stochastic optimization, as described in the rest of this section. The following notation is used: index $n \in \mathcal{N} = \{1, \dots, N_{\text{bus}}\}$ denotes the grid node among total N_{bus} nodes, $l \in \mathcal{L} = \{1, \dots, L\}$ denotes the line index, and $\mathcal{T} = \{t, t+1, \dots, t+T\}$ denotes the time index (with interval duration Δt).

2.1. Cost function

2.1.1. Investment costs for ESSs

Let $E_n^{\text{ess}} \in \mathbb{R}^+$ and $P_n^{\text{ess}} \in \mathbb{R}^+$ denote the energy capacity of a ESS at node n and the rated power of its converter, respectively (one, possibly aggregated, ESS per node is assumed). The binary variable $F_n^{\text{ess}} \in \{0, 1\}$ indicate whether a ESS is installed at node n. The investment costs for installing a ESS with energy capacity E_n^{ess} and power rating P_n^{ess} is:

$$J^I\left(P_n^{\text{ess}}, E_n^{\text{ess}}, F_n^{\text{ess}}\right) = C^{\text{P}} P_n^{\text{ess}} + C^{\text{E}} E_n^{\text{ess}} + C^{\text{F}} F_n^{\text{ess}}, \tag{1}$$

where C^{P}, C^{E} and C^{F} are the unitary cost for rated power, unitary cost for energy capacity and installation cost, respectively.

It is worth highlighting that degradation costs are not included in this analysis because, in this application, batteries are used to mitigate the effects of the daily peaks of PV generation, and the number of cycles does not result in a significant cycle aging compared to calendar aging ([1]).

[1] This hypothesis was corroborated by performing a rainflow counting analysis on the battery power found by the proposed optimal power flow. This resulted in 1.5 equivalent cycles per day. Considering a cycle life of 8'000 and 20'000 cycles for lithium-iron-phosphate and lithium-titanate-oxide electrochemistry (technologies typically adopted in grid application), respectively, the battery service life would be 15 and 36 years, respectively, thus not dominant compared to calendar life due to calendar aging (typically 15–20 years).

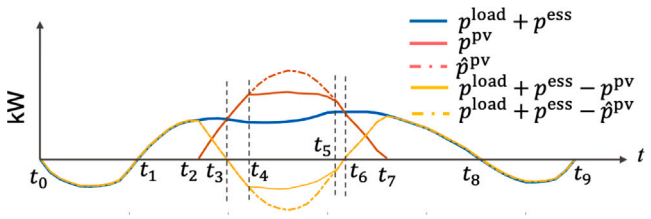

Fig. 1. Example of nodal aggregated contributions of PV power, ESS power and load.

2.1.2. Operational costs

The cost (or revenue, if negative) for operating energy storage is given by buying and selling electricity to the grid operator. Electricity is purchased from the grid at the retail electricity price c_t^{im} and sold at the wholesale electricity price c_t^{ex}. Let $p_{n,t}^{\text{im}}$ and $p_{n,t}^{\text{ex}}$ be the nodal imported and exported power at time t and node n. The operational cost is then:

$$J_{n,t}^{OP} = p_{n,t}^{\text{im}} c_t^{\text{im}} - p_{n,t}^{\text{ex}} c_t^{\text{ex}}. \tag{2}$$

Nodal power export and import depend on PV generation, ESSs' power, and nodal demand. For example, Fig. 1 shows the load ($p_{n,t}^{\text{load}}$), PV power potential ($\hat{p}_{n,t}^{\text{pv}}$), actual (curtailed) PV power ($p_{n,t}^{\text{pv}}$), and ESS power ($p_{n,t}^{\text{ess}}$). In this example, the node exports power from t_0 to t_1, t_3 to t_6, and t_8 to t_9. PV generation is consumed locally between t_2 and t_7 and is curtailed between t_4 and t_5. The imported and exported electricity at node n and time t is modeled as:

$$p_{n,t}^{\text{im}} = [p_{n,t}^{\text{load}} + p_{n,t}^{\text{ess}} - p_{n,t}^{\text{pv}}]^+ \tag{3}$$

$$p_{n,t}^{\text{ex}} = [-(p_{n,t}^{\text{load}} + p_{n,t}^{\text{ess}} - p_{n,t}^{\text{pv}})]^+ \tag{4}$$

where $[x]^+ = \max(x, 0)$ is the positive part operator. The operational cost is then:

$$J_{n,t}^{OP}(p_{n,t}^{\text{pv}}, p_{n,t}^{\text{ess}}) = [p_{n,t}^{\text{load}} + p_{n,t}^{\text{ess}} - p_{n,t}^{\text{pv}}]^+ c_t^{\text{im}} - [-(p_{n,t}^{\text{load}} + p_{n,t}^{\text{ess}} - p_{n,t}^{\text{pv}})]^+ c_t^{\text{ex}}. \tag{5}$$

As illustrated in Appendix A, the expression above can be reformulated as:

$$J_{n,t}^{OP}(p_{n,t}^{\text{pv}}, p_{n,t}^{\text{ess}}) = (c_t^{\text{im}} - c_t^{\text{ex}})[p_{n,t}^{\text{pv}} - p_{n,t}^{\text{load}} - p_{n,t}^{\text{ess}}]^+ + c_t^{\text{im}} \left(p_{n,t}^{\text{load}} + p_{n,t}^{\text{ess}} - p_{n,t}^{\text{pv}}\right). \tag{6}$$

which is a positive weighted sum of two convex functions (thus convex) provided that $c_t^{\text{im}} \geq c_t^{\text{ex}}$ ([2]).

2.2. Constraints

2.2.1. Grid model

We consider a balanced and transposed three-phase system modeled by its single-phase equivalent. Grid constraints are represented with a linearized grid model computed with the sensitivity coefficient method described in [2,24]. Computing the sensitivity coefficients requires solving a system of linear equations as a function of the grid state and admittance matrix [24,25], whose solution is guaranteed to exist and be unique when the Jacobian of the load flow problem is locally invertible [26].

The active and reactive power at the grid connection point (GCP) of this distribution grid with the upper-grid level is denoted by $p_t^{\text{gcp}}, q_t^{\text{gcp}} \in \mathbb{R}$. Nodal voltages and lines current magnitudes are denoted by vectors $|\mathbf{v}_t| \in \mathbb{R}^{|\mathcal{N}|}$ and $|\mathbf{i}_t| \in \mathbb{R}^{|\mathcal{L}|}$ at time index t. The bold-typeface represents vectors. Symbols $\mathbf{p}_t^{\text{pv}}, \mathbf{p}_t^{\text{load}}$, $\mathbf{p}_t^{\text{ess}}$ and $\mathbf{q}_t^{\text{pv}}, \mathbf{q}_t^{\text{load}}$, $\mathbf{q}_t^{\text{ess}}$ collect aggregated active and reactive power injections of PV power, ESS power, and load,

[2] This is normally the case as the retail electricity price is typically larger than the wholesale electricity price due to grid tariffs.

respectively. In this setting, active and reactive nodal injections at time t read as:

$$\mathbf{p}_t = \mathbf{p}_t^{\text{pv}} - \mathbf{p}_t^{\text{load}} - \mathbf{p}_t^{\text{ess}} \qquad t \in \mathcal{T} \tag{7}$$

$$\mathbf{q}_t = \mathbf{p}_t^{\text{pv}} - \mathbf{q}_t^{\text{load}} - \mathbf{q}_t^{\text{ess}} \qquad t \in \mathcal{T}. \tag{8}$$

Linearized grid quantities as a function of the nodal injections and the grid states (dependency on the grid admittance matrix and grid operating point are omitted to simplify the notation) are

$$|\mathbf{v}_t| = \boldsymbol{\Phi}^{\mathbf{v}}(\mathbf{p}_t, \mathbf{q}_t, |\mathbf{v}_0|) = \mathbf{A}_t^{\mathbf{v}} \begin{bmatrix} \mathbf{p}_t \\ \mathbf{q}_t \end{bmatrix} + \mathbf{b}_t^{\mathbf{v}} \tag{9a}$$

$$|\mathbf{i}_t| = \boldsymbol{\Phi}^{\mathbf{i}}(\mathbf{p}_t, \mathbf{q}_t, |\mathbf{v}_0|) = \mathbf{A}_t^{\mathbf{i}} \begin{bmatrix} \mathbf{p}_t \\ \mathbf{q}_t \end{bmatrix} + \mathbf{b}_t^{\mathbf{i}} \tag{9b}$$

$$\begin{bmatrix} p_t^{\text{gcp}} \\ q_t^{\text{gcp}} \end{bmatrix} = \boldsymbol{\Phi}^{\mathbf{s}}(\mathbf{p}_t, \mathbf{q}_t, \tilde{s}_0) = \mathbf{A}_t^{\text{gcp}} \begin{bmatrix} \mathbf{p}_t \\ \mathbf{q}_t \end{bmatrix} + \mathbf{b}_t^{\text{gcp}} \tag{9c}$$

where $\mathbf{A}_t^{\mathbf{v}} \in \mathbb{R}^{|\mathcal{N}|\times 2|\mathcal{N}|}$ and $\mathbf{b}_t^{\mathbf{v}} \in \mathbb{R}^{|\mathcal{N}|}$, $\mathbf{A}_t^{\mathbf{i}} \in \mathbb{R}^{|\mathcal{L}|\times 2|\mathcal{N}|}$ and $\mathbf{b}_t^{\mathbf{i}} \in \mathbb{R}^{|\mathcal{L}|}$, $\mathbf{A}_t^{\text{gcp}} \in \mathbb{R}^{2\times 2|\mathcal{N}|}$ and $\mathbf{b}_t^{\text{gcp}} \in \mathbb{R}^2$ collect the sensitivity coefficients and known terms of the linear model as described in [27]. For more compact expressions, we denote the linear models of voltage and current and the power at the GCP with the functions $\boldsymbol{\Phi}^{\mathbf{v}}(\mathbf{p}_t, \mathbf{q}_t, |\mathbf{v}_0|)$, $\boldsymbol{\Phi}^{\mathbf{i}}(\mathbf{p}_t, \mathbf{q}_t, |\mathbf{v}_0|)$ and $\boldsymbol{\Phi}^{\mathbf{s}}(\mathbf{p}_t, \mathbf{q}_t, \tilde{s}_0)$, respectively. Here, $\mathbf{v}_0$ and $\tilde{s}_0$ are the initial operating point for power-flow linearization of voltage and power at the GCP.

The grid constraints read as:

$$\underline{\mathbf{v}} \le \boldsymbol{\Phi}^{\mathbf{v}}(\mathbf{p}_t, \mathbf{q}_t, |\mathbf{v}_0|) \le \overline{\mathbf{v}} \qquad t \in \mathcal{T} \tag{10a}$$

$$0 \le \boldsymbol{\Phi}^{\mathbf{i}}(\mathbf{p}_t, \mathbf{q}_t, |\mathbf{v}_0|) \le \bar{\mathbf{i}} \qquad t \in \mathcal{T} \tag{10b}$$

$$0 \le (p_t^{\text{gcp}})^2 + (q_t^{\text{gcp}})^2 \le \overline{S}^2 \qquad t \in \mathcal{T}, \tag{10c}$$

where $(\underline{\mathbf{v}}, \overline{\mathbf{v}})$ denotes the operational limits on the nodal voltages, $\bar{\mathbf{i}}$ the lines' ampacity and $\overline{S}$ the substation transformer capacity. The linear grid model in (9) is validated in Appendix B showing that the error on the modeling of the nodal voltages and branch currents are in the order of 10^{-6} and 10^{-3}, respectively.

2.2.2. PV generation model

PV plants's production depends on specific local weather variables and conditions. We model the PV generation potential as a function of the local plane-of-array (POA) irradiance corrected accounting for the estimated model temperature and plant rated power, as in [28]. The PV generation potential $\hat{p}_{n,t}^{\text{pv}}$ for a plant with rated power P_n^{pv} is:

$$\hat{p}_{n,t}^{\text{pv}} = I_t \left[1 + \alpha(T_t^{\text{air}} + \beta I_t - 25)\right] P_n^{\text{pv}} \tag{11}$$

where I_t is the POA irradiance, T_t^{air} the air temperature, $\alpha = -0.0043$ and $\beta = 0.038$ are empirical parameters for open-rack PV plants [28]. POA irradiance can be computed for arbitrary tilt and azimuth configurations of PV panels by applying transposition models to global horizontal irradiance (GHI) measurements, which are commonly available from pyranometers measurements, satellite estimations, or statistical data. Air temperature is also accessible from historical measurements/statistics.

We model curtailable PV plants as controllable resources operating between 0 kW and the generation potential (11):

$$0 \le p_{n,t}^{\text{pv}} \le \hat{p}_{n,t}^{\text{pv}}. \tag{12}$$

where $p_{n,t}^{\text{pv}}$ is the aggregated PV generation at node n and is a variable of the proposed method. PV power plants can also inject reactive power, and thus feature an additional constraint on the capability curve of the PV power converter. However, plants are here assumed to operate at a unitary power factor, as it normally happens for small/medium scale PV facilities connected to distribution grids.

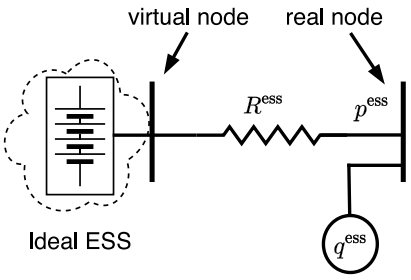

Fig. 2. Equivalent circuit model of ESS.

2.2.3. ESS operations

We model ESS operations as controllable active and reactive power injections, $p_{n,t}^{\text{ess}}$ and $q_{n,t}^{\text{ess}}$, subject to converters' capability curve and state-of-energy requirements. The first constraint reads as:

$$0 \le (p_{n,t}^{\text{ess}})^2 + (q_{n,t}^{\text{ess}})^2 \le (P_n^{\text{ess}})^2. \tag{13a}$$

This convex expression is approximated with a piecewise linearization to retain the linearity of the constraints, as proposed in [3]. The evolution of the ESS state-of-energy (SOE) is modeled as

$$\text{SOE}_{n,t+1} = \text{SOE}_{n,t} - p_{n,t}^{\text{ess}} \Delta t, \tag{13b}$$

where Δt is the sampling time. ESS' charging and discharging losses are accounted for by augmenting the load flow problem formulation with virtual transmission lines represented by an equivalent resistance (as shown in Fig. 2) designed to reproduce ESS's losses as proposed in [29]. This avoids introducing binary variables or other kinds of relaxations to keep track of the charging and discharging state of the ESSs. Since the ESS' resistance depends on the power and energy capacities, which are decision variables in the optimization problem, the optimization problem is solved iteratively. More information on the choice of ESS resistance is given in Appendix C. The SOE constraints are:

$$a E_n^{\text{ess}} \le \text{SOE}_{n,t} \le (1-a) E_n^{\text{ess}} \tag{13c}$$

where $0 \le a \le 0.5$ is an adjustable parameter and E_n^{ess} is the ESS energy capacity.

2.2.4. ESS installation variables

The binary variables F_n^{ess} are linked to the energy capacity and rated power of the ESS in the following way:

$$F_n^{\text{ess}} \underline{P}_n^{\text{ess}} \le P_n^{\text{ess}} \le F_n^{\text{ess}} \overline{P}_n^{\text{ess}} \tag{13d}$$

$$F_n^{\text{ess}} \underline{E}_n^{\text{ess}} \le E_n^{\text{ess}} \le F_n^{\text{ess}} \overline{E}_n^{\text{ess}}, \tag{13e}$$

where $\underline{E}_n^{\text{ess}}, \overline{E}_n^{\text{ess}}$ and $\underline{P}_n^{\text{ess}}, \overline{P}_n^{\text{ess}}$ are customizable parameters that can be used to specify the allowable ranges of energy capacity and power rating according to, for example, space availability or land use constraints.

2.3. Formulation of the planning problem

The decision variables of the problem are, on the one hand, the sites, power rating, energy capacity, and charge/discharge of the ESSs, and, on the other hand, the PV production adjusted for curtailment at all the nodes of the grid. Decision variables are collected in the set $\chi = \left\{ P_n^{\text{ess}}, E_n^{\text{ess}} \in \mathbb{R}^+, F_n^{\text{ess}} \in \{0,1\}, p_{n,t}^{\text{pv}}, p_{n,t}^{\text{ess}}, q_{n,t}^{\text{ess}}, \forall n \in \mathcal{N}, t \in \mathcal{T} \right\}$. Considering a planning horizon of n_y years, the ESS planning problem is

$$\min_{\chi} \sum_{n\in\mathcal{N}} J^I \left(P_n^{\text{ess}}, E_n^{\text{ess}}, F_n^{\text{ess}}\right) + \sum_{y=1}^{n_y} \sum_{t\in\mathcal{T}} \sum_{n\in\mathcal{N}} J_{n,t}^{OP}(p_{n,t}^{\text{pv}}, p_{n,t}^{\text{ess}}), \tag{14}$$

subject to:

(10), (12), (13). (15)

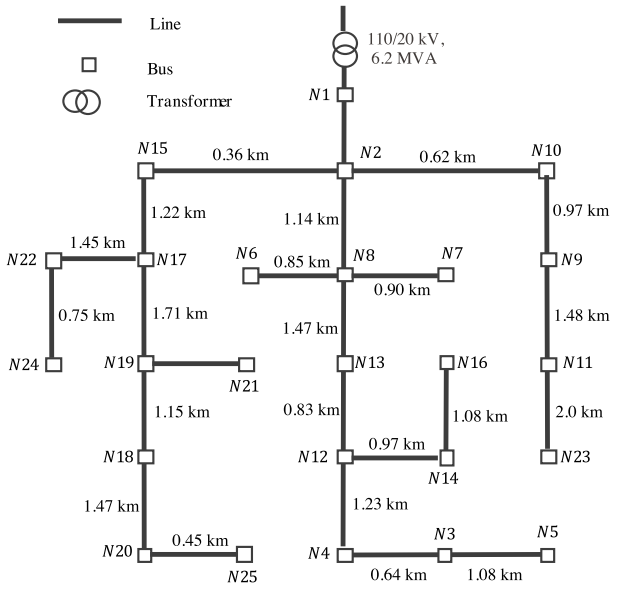

Fig. 3. Network topology corresponding to "MV1" grid of the open-data set in [20].

Table 1
Nominal load and PV per node.

Node	Load [MW]	PV [MWp]	Node	Load [MW]	PV [MWp]
N1	–	–	N14	0.17	–
N2	–	–	N15	0.18	–
N3	0.22	–	N16	0.19	–
N4	0.15	–	N17	0.17	–
N5	0.14	–	N18	0.20	–
N6	0.21	0.46	N19	0.21	–
N7	0.17	0.11	N20	0.22	–
N8	0.19	–	N21	0.16	–
N9	0.20	2.33	N22	0.18	–
N10	0.19	1.40	N23	0.26	3.61
N11	0.14	–	N24	0.23	–
N12	0.17	–	N25	0.02	–
N13	0.17	–			
			Total	**4.13**	**7.91**

The optimization problem above is a mixed integer linear program (MILP) and it can be solved using any off-the-shelf solver.

3. Simulation setup

3.1. Case study

The proposed planning scheme is applied to a medium voltage system. Network data correspond to the "MV1" grid of the open-data([3]) set in [20]. The network belongs to a region with high yearly insulation and large PV generation potential, thus possibly subject to violations of operational grid constraints due to excess production. The network topology is shown in Fig. 3. It has identical lines of ampacities 284 Amps. It is a 24-node system with voltage and power ratings of 20 kV and 6.2 MVA, respectively. The nominal loads and transformer rating is shown in Table 1. The network has a peak demand of 4.13 MW. Table 1 also shows the installed capacity of PV generation in the grid. These values of installed capacity are computed with the hosting capacity tool in [20] and correspond to the highest amount of PV generation that does not violate the operational constraints of that grid. The method is briefly described in Appendix D. For this case study, the

[3] https://go.epfl.ch/SwissMVNetworkDB

Table 2
ESS unitary costs.

Component	Units	Value
ESS converter rating (C^{P})	[CHF/MVA]	200,000
ESS energy capacity (C^{E})	[CHF/MWh]	300,000
ESS installation costs (C^{F})	[CHF/site]	100,000

Table 3
Breakdown of electricity prices for Switzerland.

Cost breakdown	Value ($\times 10^{-2}$ CHF)	% of base price
Electricity base price	7.00	100
Network utilization	10.50	150
Duties	0.63	9
Feed-in remuneration	2.45	35
Total	20.58	294

PV generation hosting capacity of this grid is 7.91 MW (without any ESSs or curtailment). In the next section, this configuration is assumed as the base case and is denoted by "100% of hosting capacity". We also define three other cases, called A, B and C that correspond to an installed PV capacity of 11.88 MWp, 15.83 MWp and 19.79 MWp (i.e. 150%, 200% and 250% of the hosting capacity), respectively. We use these cases to simulate different PV targets in the ESS sizing problem with an aim to obtain a sensitivity analysis.

3.2. PV generation and loads

The planning algorithm requires scenarios of daily electricity demand, irradiance, and the electricity prices. These values are from historical measurements of a real MV distribution network in Aigle, Switzerland. To reduce the computational burden, we cluster irradiance and load measurements and select eight scenarios[4] representative of seasonal and weekend/weekdays trends.

The load and the GHI scenarios (in pu) are shown in Fig. 4. The load profiles for the different nodes of the grid are determined by multiplying the nominal nodal demand from Table 1 with the load scenarios of Fig. 4(a). The PV generation profiles are determined by the PV model described in Section 2.2.2.

3.3. Energy storage and electricity costs

The considered unitary costs of ESS are reported in Table 2. They are derived from current market figures.

Export electricity prices are modeled using the wholesale electricity prices of the days of the selected load/GHI profiles, shown in Fig. 5. Because this paper's objective is to evaluate the economic viability of energy storage for congestion management and voltage regulation requirements resulting from installing distributed PV generation, the dynamic electricity price is replaced by its average throughout the day; in this setting, the price is constant, and ESSs have no incentives in discharging with high electricity prices and charging with low prices (energy arbitrage). The retail (import) electricity prices are obtained by adding to export electricity price the network transport charges and taxes, reported in Table 3. These values are obtained from Swiss electricity market platform([5]).

[4] As the scenario reduction is not the main focus of this paper, we work under the assumption that these scenarios represent the whole set of data. In out future work, we could use an advanced scenario reduction scheme for example in [30] guaranteeing equivalence between the reduced and complete data set.

[5] https://www.strompreis.elcom.admin.ch/

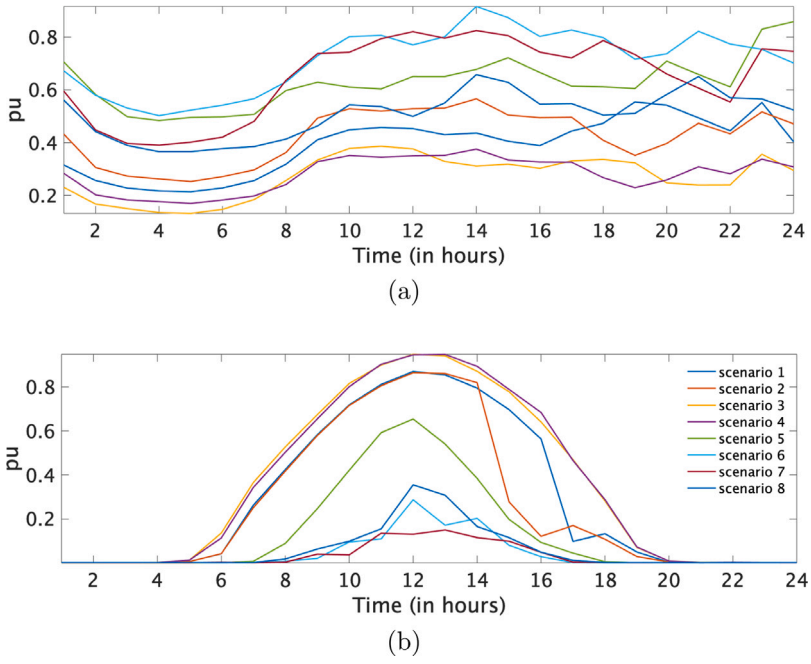

Fig. 4. Reduced scenario set for the sizing simulation: (a) Load scenarios and (b) GHI scenarios.

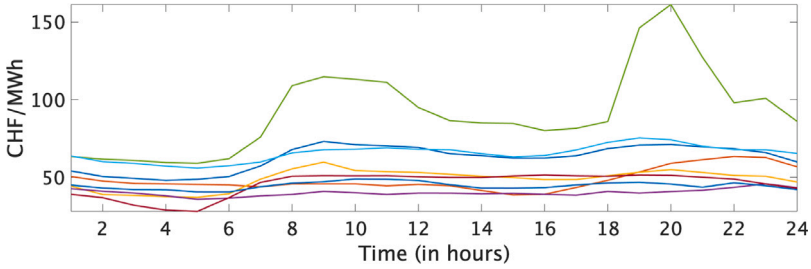

Fig. 5. Electricity price profiles for 8 typical days.

Table 4
ESS sizes without PV curtailment.

Cases	PV	ESS sizes	
	(MWp)	MW	MWh
A (150% of hosting capacity)	11.88	3.70	16.91
B (200% of hosting capacity)	15.83	7.37	43.18
C (250% of hosting capacity)	19.79	11.06	72.52

Table 5
Total ESS sizes with PV curtailment.

Cases	PV	Total ESS		PV curtailment	
	(MWp)	(MW)	(MWh)	(MWh)	(%)
A (150% of hosting capacity)	11.88	2.96	4.35	32.38	7.41
B (200% of hosting capacity)	15.83	3.02	5.12	120.29	20.87
C (250% of hosting capacity)	19.79	3.40	5.78	221.97	30.83

4. Results

The optimization problem is implemented in MATLAB with Yalmip package [31]. We used a commercial solver Gurobi [32] for solving the optimization problem. The optimization problem is run on a Macbook pro with a 2.7 GHz Quad-core intel core i7 configuration.

4.1. Sizing results

Table 4 shows the planning results without PV curtailment. It can be seen that ESS size requirements increase steadily from case A to C. This is due to increased levels of PV production results in more severe violations of the grid's constraints, finally requiring larger ESS capacity to ensure correct grid operations.

Table 5 shows the planning results with the PV curtailment option. Compared to Table 4, it can be seen that the size of the installed ESSs increases marginally from cases A to C, while the PV curtailment rises steeply. In Table 5, the percentage of PV curtailment is defined as the ratio between the curtailed PV energy and its total generation potential.

These results indicate that resorting to PV curtailment is ultimately cheaper than installing ESSs. However, the non-zero ESS capacity still allocated by the problem denotes that using ESS is still necessary to achieve cost optimality. In order to investigate more this effect, a sensitivity of the sizing requirements with respect to the cost of electricity will be presented in 4.2.

Table 6 shows the optimal sizes and sites for case A (150% of hosting capacity) with PV curtailment. Installation of ESSs is allowed at all grid nodes; however, only 4 nodes are chosen as the optimal locations.

Fig. 6 shows the power profiles of PV generation, load and ESSs power for a single scenario with and without PV curtailment. In both the cases, ESSs discharge during the morning and evening periods to supply demand, and charge in the central part of the day to absorb PV generation. With PV curtailment, PV generation is curtailed in the central hours of the day.

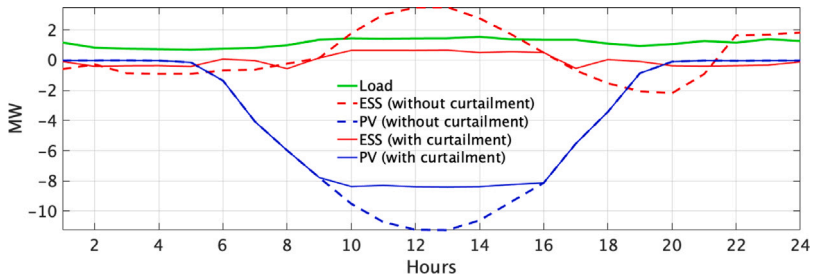

Fig. 6. Net aggregated power (MW) by the PV generation, ESS and demand with and without curtailment shown in solid and dashed line for case A.

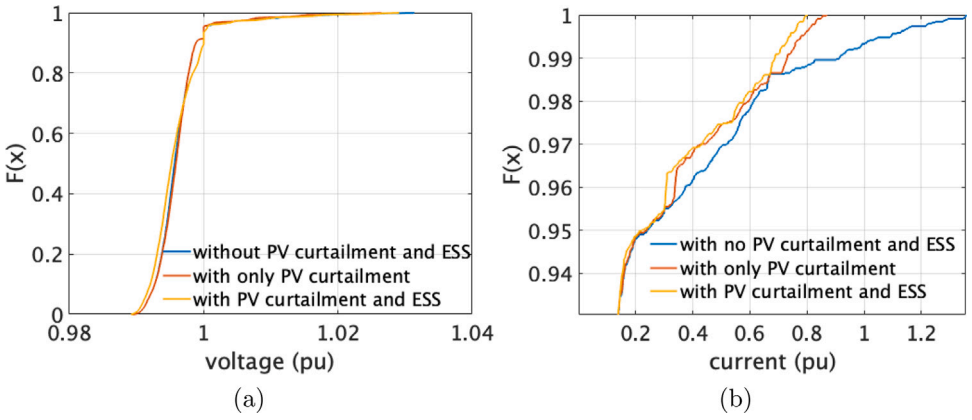

Fig. 7. CDF plots for (a) nodal voltages and (b) lines currents (in pu) for different sizing schemes.

Table 6
Optimal decisions of ESS sizes and sites for case A (with PV curtailment).

	ESS	
Sites	(MW)	(MWh)
N6	0.33	0.38
N10	0.89	1.49
N11	0.99	1.08
N23	0.75	1.40
Total	2.96	4.35

Fig. 7 shows the cumulative distribution function (CDF) of all voltages and currents for all the timesteps, scenarios and nodes/lines. These results are obtained by playing back the injections from the optimization into a nonlinear load flow ([6]). Three cases are shown: both the curtailment and ESS actions are considered (yellow line), only the PV curtailment action is considered (orange), none of the two actions are retained (blue). It can be seen that when both ESSs' and curtailment actions are activated, lines ampacity (whose limits are set at 0.8 pu in the optimization problem) are respected tightly. Removing the ESSs' injections from the problem leads to mild infeasibility of the line current limits, and removing curtailment actions too leads to severe overcurrents. Nodal voltage magnitudes feature similar behaviors in all these cases, denoting that the critical bottleneck of this power grid is the lines currents.

Table 7 compares the total objective cost in (14) for case A. It shows higher costs when PV curtailment is not considered in the planning problem.

[6] To verify the accuracy of linearized grid model in (9), we run non-linear AC power flow (using Newton Raphson's method) where the power setpoints from the newly sized ESS and PV are imposed as power injections.

Table 7
Cost comparison for case A (with 11.8MWp PV).

	ESS without PV curtailment	ESS with PV curtailment
ESS Investment (CHF) $\times 10^6$	6.11	2.29
Electricity (export) (CHF) $\times 10^6$	12.33	11.75
Electricity (import) (CHF) $\times 10^6$	46.36	36.75
Total cost (CHF) $\times 10^6$	40.14	27.28

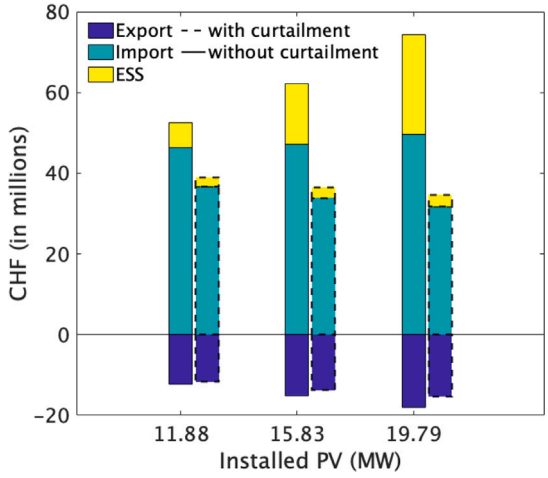

Fig. 8. Cost (Investment and electricity costs combined) comparison between planning with and without PV curtailments.

Fig. 8 extends this analysis to the different cases (A, B and C) of installed PV capacity. It shows that including curtailment in the planning problem achieves the lowest costs.

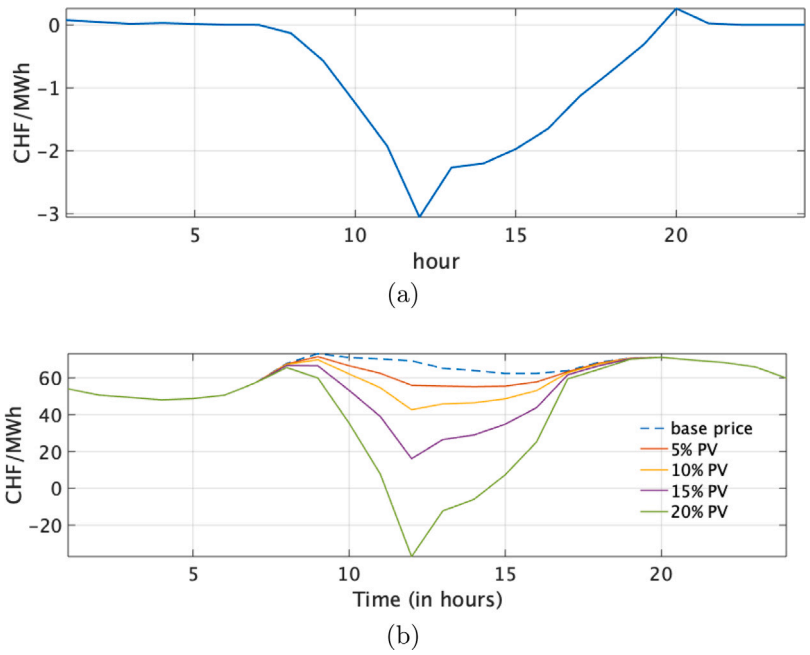

Fig. 9. Impact of PV (in the generation mix) on electricity prices: (a) electricity price change per % PV injection and (b) electricity price with different PV scenarios.

4.2. Impact of electricity prices on ESS sizing

Because the economic viability of ESS is given in this paper by storing and selling (otherwise curtailed) PV generation, it is interesting to investigate the impact of the selling electricity price on the sizing results.

In power system scenarios with significant levels of installed PV generation capacity, higher or lower levels of PV generation in the global energy mix can impact the electricity price.

The authors of [33] have modeled this effect and estimated the electricity price as a function of PV generation from data from the German and Austrian electricity markets. Based on this model and assuming similar price dynamics in Switzerland, we estimate the price evolution using the following linear expression

$$\tilde{c}_t^{\mathrm{ex}} = c_t^{\mathrm{ex}} + \hat{p}_t^{\mathrm{pv}} \Delta c_t^{\mathrm{ex}} P_{\mathrm{swiss}}^{\mathrm{pv\%}} \tag{16}$$

where Δc^{ex} (whose value is shown in Fig. 9(a)) is the change in electricity price due to a 1% increase of PV generation in the countrywide generation mix, and $P_{\mathrm{swiss}}^{\mathrm{pv\%}}$ is the percentage of PV generation in the countrywide generation mix. The resulting electricity prices for different proportions (5%–20%) of installed PV generation capacity in Switzerland is shown in Fig. 9(b). For computing the ESS sizes under different levels of installed PV generation capacity, we consider the averaged electricity price in each case of Fig. 9(b).

Table 8 shows the ESS sizes (MW/MWh) and curtailment with different price scenarios ($P_1 - P_5$) corresponding to different level of PV penetration (3 - 24GWp) at the country scale. It can be seen that the electricity price influences the sizes of the ESS installed in the grid. Compared to the base case (scenario P_1), scenario P_5 results in a significant reduction of the ESS size (50%, approximately). The reason for this is that the drop in the electricity prices reduced the revenue from the exported electricity prices, consequently reducing the investment in the ESS.

4.3. Impact of ESS costs on sizing

Cost of energy storage technologies (such as batteries and power-to-x energy storage technologies) are projected to decrease in the future [34]. Table 9 shows the sizing results for ESS costs from 10% to 100% of the cost figures assumed in the former results. As evident from the comparison, lower costs lead to larger ESS sizes, reducing PV curtailment.

Table 8
ESS sizes (for case A) with changing electricity price.

Countrywide PV scenarios			Export price	ESS sizes		PV curtailed
Label	$P_{\mathrm{swiss}}^{\mathrm{pv\%}}$(%)	GWp	CHF/MWh	MW	MWh	%
P_1	0	0	62.6	2.96	4.35	7.41
P_2	5	3	60.2	2.91	4.30	7.45
P_3	10	6	55.3	2.52	3.97	7.89
P_4	20	12	50.4	2.20	3.57	8.42
P_5	40	24	43.0	0.58	1.10	11.14

Table 9
ESS sizes (for case A) with varying ESS reservoir costs.

ESS cost	ESS sizes		PV curtailed
Scaling factor	MW	MWh	%
0.1	4.87	8.58	3.38
0.5	3.70	5.90	6.21
1	2.96	4.35	7.41

5. Conclusions

This work developed a planning tool for cost-optimally siting and sizing energy storage systems considering the option of curtailable installed PV production to respect the operational constraints of the power grid. The key addressed question is whether it is more economical to curtail PV generation as opposed to installing ESSs in the network. The methodology is a cost optimization problem that maximizes the revenues of selling electricity to the grid minus the capital investment for the ESS over a given planning horizon subject to grid constraints, modeled using a linearized grid model based on sensitivity coefficients. Energy storage provides active and reactive power compensation in case of overproduction of the PV generation.

Results showed that curtailing PV generation is cheaper than installing batteries. A sensitivity analysis showed that decreasing costs of energy storage technologies could make installing energy storage cost-competitive compared to curtailing PV generation.

CRediT authorship contribution statement

Rahul Gupta: Conceptualization, Methodology, Software, Validation, Visualization, Writing – original draft. **Fabrizio Sossan:** Conceptualization, Validation, Supervision, Writing – review & editing, Resources, Project administration.

Declaration of competing interest

The authors declare that they have no known competing financial interests or personal relationships that could have appeared to influence the work reported in this paper.

Data availability

Data will be made available on request.

Appendix A. Reformulation of the non-convex cost function

The cost function:

$$J^{\mathrm{OP}}(x) = [x]^{+} c_t^{\mathrm{im}} - [-x]^{+} c_t^{\mathrm{ex}} \tag{A.1}$$

is non-convex because it is the difference of two convex functions. Since $[x]^{+} = x + [-x]^{+}$, replacing it in (A.1) yields:

$$J^{\mathrm{OP}}(x) = (x + [-x]^{+}) c_t^{\mathrm{im}} - [-x]^{+} c_t^{\mathrm{ex}} = \tag{A.2}$$

$$= [-x]^{+} (c_t^{\mathrm{im}} - c_t^{\mathrm{ex}}) + x c_t^{\mathrm{im}}. \tag{A.3}$$

Appendix B. Validation of the linear grid model and convergence

We validate the linear approximations of the power flow against original non-linear power flow equations. The comparison is performed in terms of the modeling of voltage and current magnitude computed by the linearized OPF model and the ones by the nonlinear true power flow. As mentioned before, linear approximations of the power flow are corrected with updated power injections of the sized ESS and PV till the optimization cost function and ESS decision settles. Fig. B.10 shows the flow diagram for convergence of the planning problem. The convergence criterion is that the planning objective does not change from one iteration to the next within a pre-defined threshold value.

Fig. B.11 shows the convergence of sizes after 4 iterations. We compute the empirical CDF plot of the voltage and current magnitude errors between the linearized model and the AC power flow. The plots in Fig. B.12 show that the error on the modeling of the voltages and currents are in the order of 10^{-6} and 10^{-3}, respectively. Thus, the linearized grid model based on sensitivity coefficients represents true power flow equations within the tolerance bound of 10^{-3} pu.

Appendix C. ESS equivalent resistance

To determine the ESS resistance, we build upon the expression derived in [29,35], the ESS equivalent resistance in per unit (p.u.) is expressed as

$$R^{\mathrm{ess}} = \frac{E_{\mathrm{loss}}^{\mathrm{ess}}}{\sum_{\mathcal{T}} (p_t^{\mathrm{ess}})^2 \Delta t} \text{ p.u.} \tag{C.1}$$

where $E_{\mathrm{loss}}^{\mathrm{ess}}$ refer to ESS losses.

Considering the equivalence between the efficiency model and resistance model, the resistance can be expressed in per unit (p.u.) we express $E_{\mathrm{loss}}^{\mathrm{ess}} = \eta E^{\mathrm{ess}}$, where η is the efficiency obtained from the ESS and converter datasheets. With this, the resistance can be expressed as

$$R^{\mathrm{ess}} = \frac{\eta E^{\mathrm{ess}}}{\sum_{\mathcal{T}} (p_t^{\mathrm{ess}})^2 \Delta t} \text{ p.u.} \tag{C.2}$$

To compute resistance valid for the worst case, i.e. when the ESS is mostly operating at the full power, we can replace p_t^{ess} by P^{ess}. Under this assumption, the resistance is

$$R^{\mathrm{ess}} = \frac{\eta E^{\mathrm{ess}}}{\sum_{\mathcal{T}} (P^{\mathrm{ess}})^2 \Delta t} = R_0^{\mathrm{ess}} \frac{E^{\mathrm{ess}}}{(P_t^{\mathrm{ess}})^2} \text{ p.u.} \tag{C.3}$$

where R_0^{ess} is a constant, predetermined using manufacturer datasheet. Using (C.3), it can be seen that ESS resistance is proportional to the ESS energy size and inversely proportional to the converter power rating. Therefore, for each iteration in the planning problem when ESS energy and converter sizes are updated, it uses (C.3) to update the resistance.

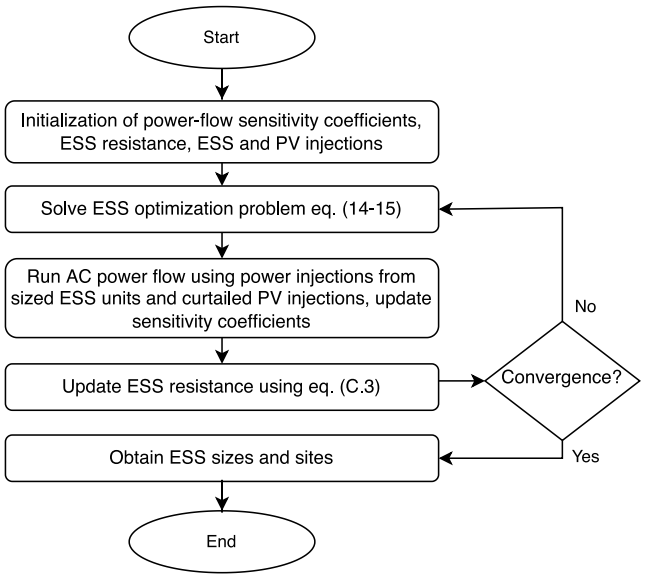

Fig. B.10. Schematic showing flow diagram of planning problem convergence.

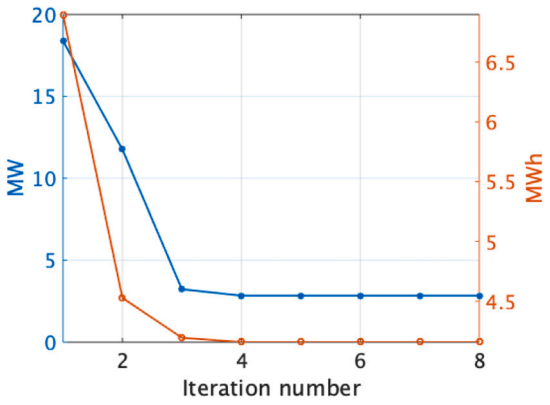

Fig. B.11. Plots showing the convergence of the ESSs power and energy sizes by correcting the linear power flow coefficients with the newest battery injections from the previous iteration.

Appendix D. PV hosting capacity computation

We use the PV hosting problem of [20] that aims to maximize the PV installation within a grid considering the limits on the nodal voltages

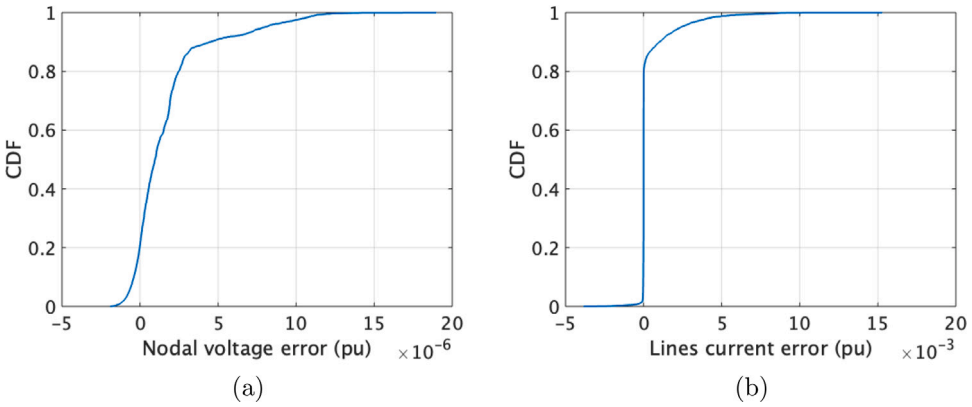

Fig. B.12. CDF plots (a) nodal voltages error and (b) branch current error.

and lines ampacities. The problem is maximizing total PV installation with decisions P_n^{pv},

$$\underset{\{P_n^{\text{pv}} \in \mathbf{R}^+, n \in \mathcal{N}\}}{\text{maximize}} \left\{ \sum_{n \in \mathcal{N}} \gamma_n P_n^{\text{pv}} \right\} \tag{D.1a}$$

where γ_n is the yearly capacity factor per location of the MV node (from PVGIS[7]) to favor locations with higher insolation conditions. This problem is solved with respect to grid's constraints modeled by linearized grid model ([2,36])

(10a), (10b), (10c) (D.1b)

$$\mathbf{p}_t = \mathbf{p}_t^{\text{pv}} - \mathbf{p}_t^{\text{load}} \qquad t \in \mathcal{T} \tag{D.1c}$$

$$\mathbf{q}_t = \mathbf{p}_t^{\text{pv}} - \mathbf{q}_t^{\text{load}} \qquad t \in \mathcal{T} \tag{D.1d}$$

and maximum allowable PV ($\overline{P}_n^{\text{pv}}$) per MV node, which is computed considering the geographical constraints of the area. The constraint reads as

$$P_n^{\text{pv}} \leq \overline{P}_n^{\text{pv}} \tag{D.1e}$$

And the final constraint is PV generation modeled using irradiance scenarios, it reads as

(12) (D.1f)

The above problem is linear and convex and can be solved efficiently with any solver.

References

[1] Liu MZ, Procopiou AT, Petrou K, Ochoa LF, Langstaff T, Harding J, et al. On the fairness of PV curtailment schemes in residential distribution networks. IEEE Trans Smart Grid 2020;11(5):4502–12.

[2] Gupta R, Sossan F, Paolone M. Grid-aware distributed model predictive control of heterogeneous resources in a distribution network: Theory and experimental validation. IEEE Trans Energy Convers 2020;36(2):1392–402.

[3] Nick M, Cherkaoui R, Paolone M. Optimal planning of distributed energy storage systems in active distribution networks embedding grid reconfiguration. IEEE Trans Power Syst 2017;33(2):1577–90.

[4] Hemmati R, Saboori H, Jirdehi MA. Stochastic planning and scheduling of energy storage systems for congestion management in electric power systems including renewable energy resources. Energy 2017;133:380–7.

[5] Novoa L, Flores R, Brouwer J. Optimal renewable generation and battery storage sizing and siting considering local transformer limits. Appl Energy 2019;256:113926.

[6] Rider M, Garcia A, Romero R. Power system transmission network expansion planning using AC model. IET Gener, Transm Distrib 2007;1(5):731–42.

[7] Hooshmand R-A, et al. Combination of AC transmission expansion planning and reactive power planning in the restructured power system. Energy Convers Manage 2012;55:26–35.

[8] Luthander R, Widén J, Munkhammar J, Lingfors D. Self-consumption enhancement and peak shaving of residential photovoltaics using storage and curtailment. Energy 2016;112:221–31.

[9] Von Appen J, Braun M. Strategic decision making of distribution network operators and investors in residential photovoltaic battery storage systems. Appl Energy 2018;230:540–50.

[10] Sevilla FRS, Parra D, Wyrsch N, Patel MK, Kienzle F, Korba P. Techno-economic analysis of battery storage and curtailment in a distribution grid with high PV penetration. J Energy Storage 2018;17:73–83.

[11] O'Shaughnessy E, Cruce JR, Xu K. Too much of a good thing? Global trends in the curtailment of solar PV. Sol Energy 2020;208:1068–77.

[12] Aziz T, Ketjoy N. PV penetration limits in low voltage networks and voltage variations. IEEE Access 2017;5:16784–92.

[13] Procopiou AT, Ochoa LF. Voltage control in PV-rich LV networks without remote monitoring. IEEE Trans Power Syst 2016;32(2):1224–36.

[14] Ricciardi TR, Petrou K, Franco JF, Ochoa LF. Defining customer export limits in PV-rich low voltage networks. IEEE Trans Power Syst 2018;34(1):87–97.

[15] Nazaripouya H, et al. Optimal sizing and placement of battery energy storage in distribution system based on solar size for voltage regulation. In: 2015 IEEE PES general meeting. IEEE; 2015, p. 1–5.

[16] Yang Y, Li H, Aichhorn A, Zheng J, Greenleaf M. Sizing strategy of distributed battery storage system with high penetration of photovoltaic for voltage regulation and peak load shaving. IEEE Trans Smart Grid 2013;5(2):982–91.

[17] Zeraati M, Golshan MEH, Guerrero JM. Distributed control of battery energy storage systems for voltage regulation in distribution networks with high PV penetration. IEEE Trans Smart Grid 2016;9(4):3582–93.

[18] Shi Y, Xu B, Wang D, Zhang B. Using battery storage for peak shaving and frequency regulation: Joint optimization for superlinear gains. IEEE Trans Power Syst 2017;33(3):2882–94.

[19] Conte F, Massucco S, Schiapparelli G-P, Silvestro F. Day-ahead and intra-day planning of integrated BESS-PV systems providing frequency regulation. IEEE Trans Sustain Energy 2019;11(3):1797–806.

[20] Gupta R, Sossan F, Paolone M. Countrywide PV hosting capacity and energy storage requirements for distribution networks: The case of Switzerland. Appl Energy 2021;281:116010.

[21] Karagiannopoulos S, Aristidou P, Ulbig A, Koch S, Hug G. Optimal planning of distribution grids considering active power curtailment and reactive power control. In: PESGM. IEEE; 2016, p. 1–5.

[22] Gan L, Li N, Topcu U, Low SH. Exact convex relaxation of optimal power flow in radial networks. IEEE Trans Automat Control 2014;60(1):72–87.

[23] Nick M, Cherkaoui R, Le Boudec J-Y, Paolone M. An exact convex formulation of the optimal power flow in radial distribution networks including transverse components. IEEE Trans Automat Control 2017;63(3):682–97.

[24] Christakou K, LeBoudec J-Y, Paolone M, Tomozei D-C. Efficient computation of sensitivity coefficients of node voltages and line currents in unbalanced radial electrical distribution networks. IEEE Trans Smart Grid 2013;4(2):741–50.

[25] Zhou Q, Bialek J. Simplified calculation of voltage and loss sensitivity factors in distribution networks. In: Proc. 16th power syst. comput. conf.. 2008.

[26] Paolone M, Le Boudec J-Y, Christakou K, Tomozei D-C. Optimal voltage control processes in active distribution networks. Technical report, The Institution of Engineering and Technology-IET; 2015.

[27] Gupta R, Sossan F, Paolone M. Performance assessment of linearized OPF-based distributed real-time predictive control. In: IEEE powertech 2019. Milan, Italy; 2019.

[7] https://re.jrc.ec.europa.eu/pvg_tools/en/tools.html

[28] Sossan F, Scolari E, Gupta R, Paolone M. Solar irradiance estimations for modeling the variability of photovoltaic generation and assessing violations of grid constraints: A comparison between satellite and pyranometers measurements with load flow simulations. J Ren Sust Energy 2019;11(5):056103.
[29] Stai E, Sossan F, Namor E, Boudec JYL, Paolone M. A receding horizon control approach for re-dispatching stochastic heterogeneous resources accounting for grid and battery losses. Electr Power Syst Res 2020;185.
[30] Yi JH, Cherkaoui R, Paolone M. Optimal allocation of ESSs in active distribution networks to achieve their dispatchability. IEEE Trans Power Syst 2020;36(3):2068–81.
[31] Lofberg J. YALMIP: A toolbox for modeling and optimization in MATLAB. In: 2004 IEEE international conference on robotics and automation (IEEE Cat. No. 04CH37508). IEEE; 2004, p. 284–9.
[32] Bixby B. The gurobi optimizer. Transp Re-Search Part B 2007;41(2):159–78.
[33] Hartner M, Permoser A. Through the valley: The impact of PV penetration levels on price volatility and resulting revenues for storage plants. Renew Energy 2018;115:1184–95.
[34] Ralon P, Taylor M, Ilas A, Diaz-Bone H, Kairies K. Electricity storage and renewables: Costs and markets to 2030. Abu Dhabi, UAE: International Renewable Energy Agency; 2017.
[35] Stai E, Reyes-Chamorro L, Sossan F, Le Boudec J-Y, Paolone M. Dispatching stochastic heterogeneous resources accounting for grid and battery losses. IEEE Trans Smart Grid 2017;9(6):6522–39.
[36] Gupta R, Fahmy S, Paolone M. Coordinated day-ahead dispatch of multiple power distribution grids hosting stochastic resources: an admm-based framework. Electr Power Syst Res 2020;212:108555.